INTERNATIONAL TABLES FOR CRYSTALLOGRAPHY

ISSN 1574-8707
it.iucr.org

Volume I, X-ray Absorption Spectroscopy and Related Techniques
ISBN: 978-1-119-43394-1

Chapter 5.6

Keywords: X-ray absorption spectroscopy; X-ray fluorescence; χ; $\mu \rightarrow \chi$; uncertainty.

Related chapters

Volume I: 2.1, 2.8, 3.14, 3.41, 3.43, 3.44, 3.46, 4.2, 4.3, 4.4, 4.6, 4.7

Extraction of χ: calibrations and limitations

Christopher T. Chantler*

School of Physics, University of Melbourne, Parkville, Victoria 3010, Australia. *Correspondence e-mail: chantler@unimelb.edu.au

This chapter is concerned with the ability to extract χ versus k from $\ln(I_0/I)$ (transmission) or from I_f/I_0 (fluorescence) versus E. Standard theory and analytical practice for X-ray absorption fine structure (XAFS) or extended X-ray absorption fine structure (EXAFS) derives χ from a wide range of experimental data and then presents the theoretical computation of $\chi(k)$ for nanostructural analysis. This remains one of the largest continuing challenges in theory and experiment for XAFS analysis. Empirical approaches have been used for many decades. Theoretical advances in understanding and measurement now permit greater investigation and insight, yet progress has perhaps been slow due to insufficient diagnostics on standard beamlines. This chapter will discuss advances, concerns and opportunities.

1. Introduction

For analysis of the pre-edge or the near-XANES region, it would be almost nonsensical to extract $\chi(k)$ versus k from $\ln(I_0/I)$ (transmission) or from I_f/I_0 (fluorescence) versus E. However, standard theory and analytical practice for XAFS or EXAFS derives $\chi(k)$ from experimental data and then presents the theoretical computation of χ to permit nanostructural fitting (Bunker, 2010, 2024*a*; Newville, 2024). Recently, some theory has shown the capacity or facility to model the whole pre-edge–edge–XANES–XAFS region and in this case it might become sensible to fit the whole $[\mu/\rho]$ rather than to extract $\chi(k)$. However, the current status and *de facto* position is to extract $\chi(k)$ and often to then transform this to $\chi(R)$ (Bunker, 2024*b*). This first transformation remains one of the largest continuing challenges in theory and experiment for XAFS analysis.

Conventionally (that is, for the past several decades), the data are collected, a pre-edge background is subtracted, including an extrapolation to above the edge, an edge jump is imputed from the data, the above-edge data are 'flattened' or normalized to a height above the edge of unity, neglecting oscillations, and typically a spline fitting extracts the χ signal from the total (Newville, 2024; Bunker, 2024*a*).

Some issues relate to this in transmission or fluorescence in particular. To be specific, the absorption coefficient is predicted and modelled by theory, not the attenuation coefficient (transmission raw data) or the fluorescence spectrum or a selection from a region of interest (fluorescence raw data; Chantler, 2024*a*). Secondly, the different experimental modalities discussed in the different chapters in this volume require corrections for systematics such as dark-current offsets, harmonics (transmission data; Abe, 2024; Ciatto *et al.*, 2024; Chantler, 2024*b*) or dead-time corrections (fluorescence data). Theory predicts a decrease above the edge of approximately $(E - E_0)^{-3}$. Raw fluorescence data often increase with energy above the edge. 'Flattening' follows a base which is constant above the edge. These change the relative structure and amplitudes of subsequent peaks in

XAFS above the edge and thus impact upon the agreement and the range of agreement of experiment with theory. Fluorescence data generate a result which, after correction for self-absorption and absorption (Bridges & Booth, 2024), has a separate overall scale factor, and this can yield a scaling of the amplitudes of XAFS peaks relative to theory, which in turn can be accommodated by an unusual overall scaling from S_0^2.

Historically, one key omission is the absence of repeated measurements and an estimate of variance or precision per datum. In other words, often measurements are not repeated and uncertainties are not collected on a point-wise basis. Then, of course, they are not propagated to $[\mu/\rho]$ or χ. Assuming that the data have been collected with a variance, precision or uncertainty estimate per datum, and that these are propagated towards an estimate of $[\mu/\rho]$ versus E or $a_i[\mu/\rho]^*_{\rm pe}[\rho t]$ versus E (Chantler, 2024*c*), then issues of scaling, background subtraction and error propagation to χ arise. Some of these propagations remain ill-defined, due in part to the variability in defining the background to be subtracted, the edge jump and the fitting or structure of the spline, yet much of this can be quantified and propagated.

Key issues relating to transmission have been presented and emphasized in Chantler (2024*b*,*c*) and so will not be represented here. Some key concepts have recently been discussed in detail and are edited and updated generally here for all measurements, with permission from Schalken & Chantler (2018) and Trevorah *et al.* (2020).

2. Transmission uncertainties in χ and the problem of interpolation

Following one of many standard pre-edge removals (Newville, 2024; Bunker, 2024*a*), the experimental data (from transmission XAS) are transformed into $\chi(E)$ by

$$\chi(E) = \frac{[\mu/\rho](E) - [\mu_0/\rho](E)}{-[\mu_0/\rho](E)}, \qquad (1)$$

where $[\mu_0/\rho]$ estimates the isolated-atom background curve.

Depending upon the formalism, this pre-processing removes background effects from a matrix and solvent and any absorption or scattering from atoms that are not involved in the edge, defines and subtracts the edge energy or edge offset E_0, removes the edge jump to the above-edge region and somehow estimates an isolated-atom absorption function above the edge. It is often incorporated into a single routine which makes an empirical spline fit through the data points above the absorption edge. This enables isolation of the XAFS oscillations to allow structural determination.

The spectrum is then converted to a function of (effective photoelectron) wavenumber k,

$$k = \frac{2\pi}{h}[2m_{\rm e}(E - E_0)]^{1/2}, \qquad (2)$$

where E_0 is an estimated 'edge energy', often taken from an empirical fit or from a metal reference.

However, the data are then 'always' interpolated onto a regularly spaced grid in k. This distorts the experimental values, point density, information content and experimental uncertainties (Islam *et al.*, 2014). The change of point spacing will skew the fit towards a different region of the spectrum, hence any additional time spent during the experiment in particular energy regions to gain high detail, high point density or high point accuracy on features of interest will effectively be lost. These issues are general in XAFS and apply to common packages, including *IFEFFIT*, *ARTEMIS*, *GNXAS* and *FDMX*, for example.

The recent package *mu2chi* (Schalken & Chantler, 2018) propagates data and uncertainty to χ without interpolation in order to transform the raw data while maintaining point density and point accuracy. This also demonstrated the effects that standard interpolation has on $\chi^2_{\rm r}$ and the consequences for the interpreted structure, and additionally suggested a new method of interpolation which preserves information content.

Numerous methods exist for interpolation. Previous work (Islam *et al.*, 2015) utilized a cubic spline approach. After the pre-edge and background have been subtracted in the conventional manner, a cubic fit with standard deviation uncertainties is made through four data points and is evaluated on a regular 0.05 Å^{-1} spaced grid, iteratively stepping through the data. Each point on the grid then has multiple fitted points with uncertainties, with the final value being determined using a weighted mean and the uncertainty being a weighted standard deviation.

This is common, but often the interpolated value will differ from the original value despite being located at the same E or k value (Fig. 1). This then does not reflect the real data, and measured outliers are often omitted by the spline, incorrectly improving the reported $\psi^2_{\rm r}$ or $\chi^2_{\rm r}$.

The recommendation is not to interpolate the experimental data onto a regular grid, but rather to interpolate the theoretical model onto the experimental data-point array. Otherwise, it is difficult to preserve the information content of the original experiment during interpolation. Experimental data points should of course be taken as at least semi-regular points in k-space; however, this is dependent upon an exact and correct determination of E_0 prior to data collection, which

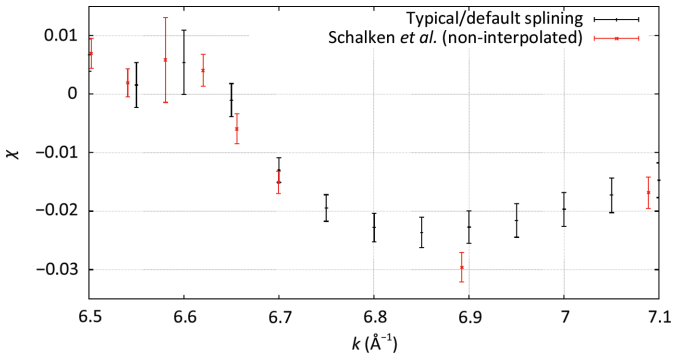

Figure 1
A typical splining method (Islam *et al.*, 2015; black) compared with the non-interpolated method (Schalken & Chantler, 2018; red). Smoothing is apparent around k = 6.9. Even when interpolated and non-interpolated approaches share a common k value, the data point differs, for example at k = 6.7. The non-interpolating approach avoids distorting the data, structure or uncertainty.

is generally implausible. Also, there can be a focus on local structure or multiple edges, which makes a more uniform scan impractical. If the experimental point density varies greatly across the fitting range, the fit will be dominated by regions of high point density. Schalken & Chantler (2018) address the question of how best to preserve the information content of a data set if it must be interpolated onto a linear grid, in this case in k-space. We have argued that in general such a grid is liable to distort features and weight spectral ranges inappropriately, and also to scale noise in the wrong way.

3. Fluorescence data-transformation issues: scaling of data, standard χ extraction limitations and processing

Care should be taken in the propagation of uncertainty when converting XAFS data from the scaled fluorescence signal I_f/I_0 or $[\mu/\rho]$ (mass absorption coefficient or mass attenuation coefficient) or μ (linear absorption coefficient) to χ, including the propagation of correlated versus uncorrelated errors and random versus systematic errors.

Almost any estimate of data uncertainty, precision or accuracy is preferred to the absence of an estimate. However, careful data collection and analysis can define these uncertainties at the 10^{-5} level compared with the active orbital magnitude of $a_i[\mu/\rho]^*_{pe}[\rho t] \simeq 0.08$–$0.12$, with an improvement of a factor of 20–200 compared with the uncorrected raw data (Trevorah *et al.*, 2020). A significant source of uncertainty is introduced in the process of converting μ to χ, an unavoidable step in the structural analysis of any XAFS data set. Perhaps the simplest and most widely used method involves background subtraction, edge estimation and fitting a spline function through the original μ data to isolate the oscillatory pattern in the XAFS data, together with glitch removal, data 'selection' and interpolation. This process (especially spline subtraction and interpolation) introduces significant error into the data set because of the unknown near-edge baseline and the common sensitivity to variations in the spline definition, which are quite difficult to quantify (Schalken & Chantler, 2018).

For fluorescence data it is common to remove Bragg glitches (monochromator secondary reflections) or sometimes to characterize them (Trevorah *et al.*, 2019). This should not be needed in a well designed transmission experiment, but appears to be inevitable in fluorescence data collection, not because of poor data, but because of the intrinsic non-cancellation of detector and monitor efficiencies. These can be characterized and corrected for, or recognized and omitted (deleted) in the determination of variance, either at some prior step or at this point in the analysis. Each of these alternatives is possible.

4. Discussion of k-weighting: estimation of additional known and unknown uncertainties and their propagation from $[\mu/\rho]$ versus E to χ, $k\chi$, $k^2\chi$ and $k^3\chi$ versus k

As noted by Krappe & Rossner (2002), 'conventional methods to obtain χ from the raw data make it very difficult to determine 'experimental' errors'. Uncertainties have been estimated and recorded during experiments for the air-path length and Kapton tape and silicon-layer thicknesses. These are key parameters in any self-absorption and attenuation correction model, and so uncertainties in these quantities lead to uncertainty in the final 'corrected' spectra.

To be clear, errors in absorption and self-absorption do not simply yield a change in the overall scale, which would cancel out when converting to χ, but an energy-dependent change, leading to different slopes in the final corrected spectra. In part, this is due in turn to uncertainties in the 'standard' extraction of χ, *i.e.* background removal, edge-energy location or definition, above-edge spline or other empirical definition of a smooth 'atomic' reference background and ergo extraction of the oscillations, amplitudes and magnitudes. Hence, an uncertainty or error, a systematic, manifests itself as a change in relative amplitude or offset in χ-versus-k space.

In, for example, Schalken & Chantler (2018), an error bar including this uncertainty was generated by producing spectra using the range of experimental lengths and thicknesses and propagating these through the χ-versus-k extraction process. This was added in quadrature to the uncertainty from averaging the pixel spectra.

This 'path-length' uncertainty could be significantly reduced by increased accuracy measurements of the experimental geometry and is not a comment on the quality of the data produced by the experiment or the relevant software package *SeAFFluX* (Trevorah *et al.*, 2019, 2020). The structural oscillations in a χ spectrum tend to decrease dramatically with increasing k, so it is common to analyse spectra scaled by k, k^2 or k^3. Fig. 2 illustrates the correct scaling of uncertainties from χ versus k to, for example, $k^2\chi$ versus k. In all cases the noise and uncertainty increase with k. This experiment was optimized in spacing and dwell time, although the beamline is second generation rather than third generation, so it remains flux-limited, especially at high k. Thus, maximal information content occurs at lower k.

A cutoff value is conventionally chosen at high k (somewhat arbitrarily) at a point where the data appear too noisy. This cutoff is enforced by a window function, most commonly a Hanning window. The methodology that we present here of propagating error bars throughout the analysis highlights a key point in the analysis methodology. The relative noise, or signal to noise, is exactly the same in all plots; however, the cutoff of the Hanning window chosen is normally fully correlated with the choice of scale (k, k^2 or k^3; Fig. 2).

With uncertainty estimates, propagation and analysis using the uncertainties, the choice of fitting on $k\chi$, $k^2\chi$ or $k^3\chi$ axes is not relevant because the fitting should be normalized by the uncertainties in all cases. Also, the higher limit of the Hanning window can then be both robust and arbitrary, because the uncertainties naturally deprecate the significance of high-k data points (Trevorah *et al.*, 2020). This methodology of error propagation then aims to accurately estimate the sources of experimental uncertainty and removes the need to arbitrarily decide on a high-k cutoff value. The lower limit of a Hanning or fitting window has a quite different origin: it usually lies in

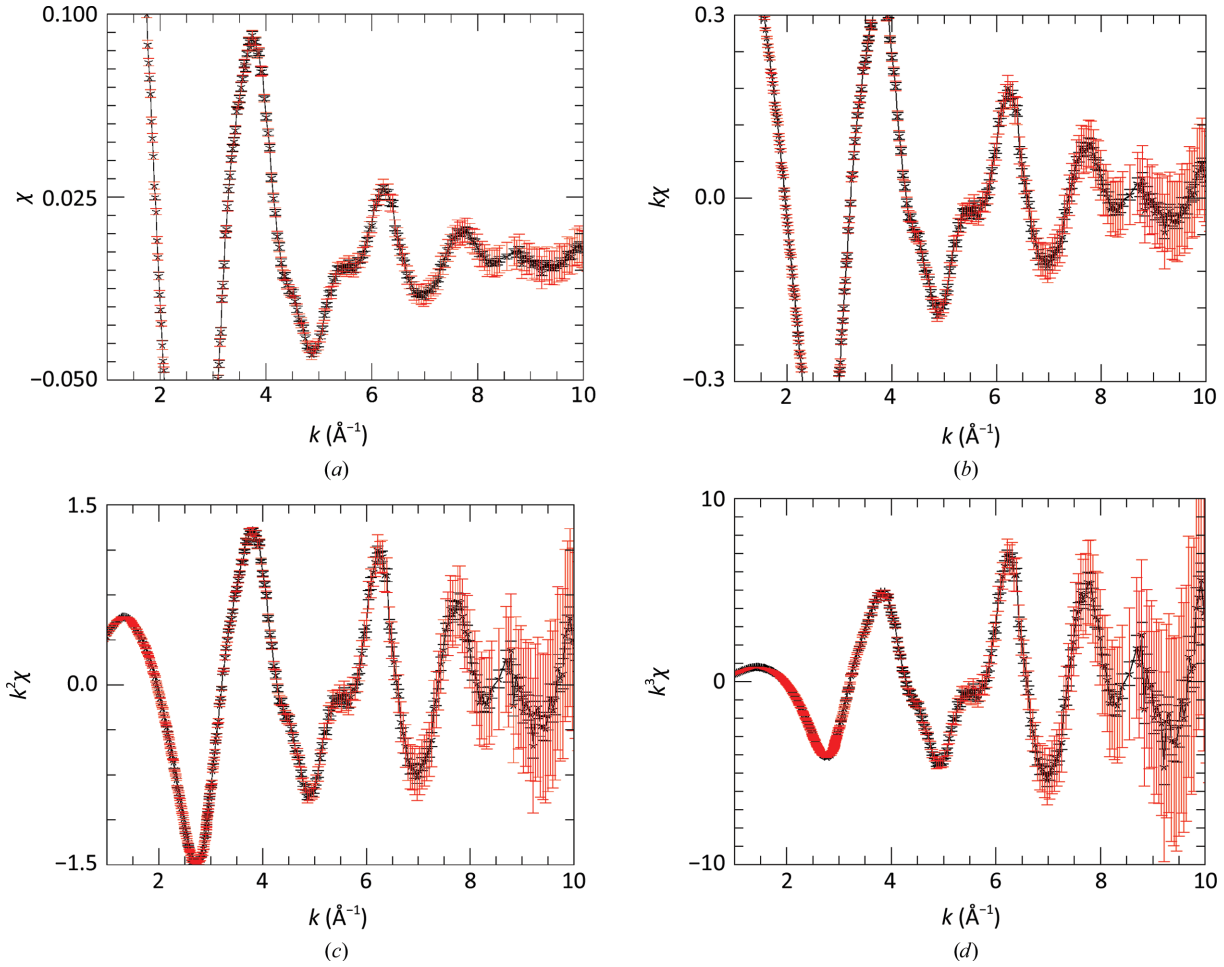

Figure 2
Plots of $k^n\chi$ versus k for fluorescence spectra. (*a*) χ versus k. (*b*) $k\chi$ versus k. (*c*) $k^2\chi$ versus k. (*d*) $k^3\chi$ versus k. The black spectrum includes the error bars from point-wise variance between pixels, whereas the red spectrum includes error bars from both point-wise variance and geometric uncertainties. The information content is highest at low k, and absolute and relative noise increases with k in a natural manner but with independent point-wise estimates.

limitations of the theory, of the model or of the parameters such as ΔE_0, and means that fitting in the low-k region yields a high χ^2_r. Avoiding these theory, model and fitting limitations implies the use of a low-k window limit for fitting. A fitting window can be used in k-space or in R-space, but the physical meaning is quite transparent in k-space.

5. Conclusion

For both transmission and fluorescence XAS, data with well defined uncertainties can be well propagated to a set of χ versus k, without interpolation, and fitted accordingly. The data sets can be sparse or dense, and the measure of significance should be valid in all cases. The recommendation is not to interpolate the experimental data onto a regular grid, but rather to interpolate the theoretical model onto the experimental data-point array. If interpolation to a regular grid is necessary, for example for transforming and fitting in R-space or for filtering and back-transforming, the recommendations of Schalken & Chantler (2018) may be used. This will help to reduce spectral distortions, reduce the limitations imposed by arbitray Hanning window limits, quantify the goodness of fit in XAFS analysis and permit further limitations to be investigated more carefully and resolved in the future.

References

Abe, H. (2024). *Int. Tables Crystallogr. I*, ch. 4.2, 594–599.
Bridges, F. & Booth, C. H. (2024). *Int. Tables Crystallogr. I*, ch. 3.44, 564–566.
Bunker, G. (2010). *Introduction to XAFS: A Practical Guide to X-ray Absorption Fine Structure Spectroscopy.* Cambridge University Press.
Bunker, G. (2024*a*). *Int. Tables Crystallogr. I*, ch. 5.2, 636–638.
Bunker, G. (2024*b*). *Int. Tables Crystallogr. I*, ch. 5.3, 639–644.
Chantler, C. T. (2024*a*). *Int. Tables Crystallogr. I*, ch. 2.8, 88–99.
Chantler, C. T. (2024*b*). *Int. Tables Crystallogr. I*, ch. 4.6, 617–623.
Chantler, C. T. (2024*c*). *Int. Tables Crystallogr. I*, ch. 4.7, 624–630.
Ciatto, G., Fonda, E. & Maurizio, C. (2024). *Int. Tables Crystallogr. I*, ch. 4.4, 606–612.
Islam, M. T., Chantler, C. T., Cheah, M. H., Tantau, L. J., Tran, C. Q. & Best, S. P. (2015). *J. Synchrotron Rad.* **22**, 1475–1491.
Islam, M. T., Tantau, L. J., Rae, N. A., Barnea, Z., Tran, C. Q. & Chantler, C. T. (2014). *J. Synchrotron Rad.* **21**, 413–423.

Krappe, H. J. & Rossner, H. H. (2002). *Phys. Rev. B*, **66**, 184303.
Newville, M. (2024). *Int. Tables Crystallogr. I*, ch. 5.1, 631–635.
Schalken, M. J. & Chantler, C. T. (2018). *J. Synchrotron Rad.* **25**, 920–934.
Trevorah, R. M., Chantler, C. T. & Schalken, M. J. (2019). *IUCrJ*, **6**, 586–602.
Trevorah, R. M., Chantler, C. T. & Schalken, M. J. (2020). *J. Phys. Chem. A*, **124**, 1634–1647.